1521-0103/365/1/140–155$35.00
THE JOURNAL OF PHARMACOLOGY AND EXPERIMENTAL THERAPEUTICS
https://doi.org/10.1124/jpet.117.244855
J Pharmacol Exp Ther 365:140–155, April 2018

The Journal of PHARMACOLOGY And Experimental Therapeutics

Development and Translational Application of a Minimal Physiologically Based Pharmacokinetic Model for a Monoclonal Antibody against Interleukin 23 (IL-23) in IL-23-Induced Psoriasis-Like Mice

Xi Chen,[1] Xiling Jiang, Rajitha Doddareddy, Brian Geist, Thomas McIntosh, William J. Jusko, Honghui Zhou, and Weirong Wang

Biologics Development Sciences, Janssen BioTherapeutics (X.C., X.J., R.D., B.G., T.M., W.W.) and Global Clinical Pharmacology (H.Z.), Janssen R&D, Spring House, Pennsylvania; and Department of Pharmaceutical Sciences, School of Pharmacy and Pharmaceutical Sciences, State University of New York at Buffalo, Buffalo, New York (W.J.J.)

Received September 21, 2017; accepted January 22, 2018

ABSTRACT

The interleukin (IL)-23/T_h17/IL-17 immune pathway has been identified to play an important role in the pathogenesis of psoriasis. Many therapeutic proteins targeting IL-23 or IL-17 are currently under development for the treatment of psoriasis. In the present study, a mechanistic pharmacokinetics (PK)/pharmacodynamics (PD) study was conducted to assess the target-binding and disposition kinetics of a monoclonal antibody (mAb), CNTO 3723, and its soluble target, mouse IL-23, in an IL-23-induced psoriasis-like mouse model. A minimal physiologically based pharmacokinetic model with target-mediated drug disposition features was developed to quantitatively assess the kinetics and interrelationship between CNTO 3723 and exogenously administered, recombinant mouse IL-23 in both serum and lesional skin site. Furthermore, translational applications of the developed model were evaluated with incorporation of human PK for ustekinumab, an anti-human IL-23/IL-12 mAb developed for treatment of psoriasis, and human disease pathophysiology information in psoriatic patients. The results agreed well with the observed clinical data for ustekinumab. Our work provides an example on how mechanism-based PK/PD modeling can be applied during early drug discovery and how preclinical data can be used for human efficacious dose projection and guide decision making during early clinical development of therapeutic proteins.

Introduction

Psoriasis is a chronic immune-mediated inflammatory skin disorder (Schön and Boehncke, 2005). Many cytokines and immune cells have been identified that promote the disease initiation and propagation (Schön and Boehncke, 2005); among these, the interleukin (IL)-23/T_h17/IL-17 immune pathways play pivotal roles (Lima and Kimball, 2010). A recent psoriasis disease model has identified IL-17 secreted by T_h17 cells as one of the key cytokines in psoriasis disease development, where T_h17 cells are activated by IL-23 (Nestle et al., 2009; Lowes et al., 2013). In psoriatic patients, both IL-23 and IL-17 exhibit elevated expression in lesional skin sites (Arican et al., 2005). There are several therapeutic monoclonal antibodies (mAbs) targeting IL-23 and IL-17 for the treatment of psoriasis, including ustekinumab, guselkumab, risankizumab, tildrazumab, secukinumab, and ixekizumab (Hu et al., 2014; Dong and Goldenberg, 2017). These biologics neutralize target cytokines at the lesional skin site, and exert anti-inflammatory activity.

Ustekinumab is an anti-IL-23/IL-12 dual therapeutic mAb that shows great therapeutic effect for the treatment of psoriasis. It neutralizes both IL-12 and IL-23 by binding to the p40 subunit shared by IL-12 and IL-23. Free cytokine suppression at target tissue sites is anticipated to drive the magnitude and duration of therapeutic effect. Albeit the pharmacokinetics (PK) of ustekinumab in serum has been well characterized and the relationship with pharmacodynamics (PD) has been established in semimechanistic PK/PD models (Zhou et al., 2010), less is known about the drug exposure at lesional skin site and its interaction with IL-23 and IL-12 therein. The aim of the present study was to develop mechanistic-based and physiologically based PK/PD models for quantitative characterization of the tissue distribution kinetics of an anti-IL-23 mAb and its IL-23-binding ability in the lesional skin site with a mouse psoriasis-like (PsL) disease model.

Mechanism-based PK/PD models contain quantitative expressions of the causal relationship between drug exposure and

[1]Current affiliation: Clinical Pharmacology and Pharmacometrics, Bristol-Myers Squibb, Princeton, New Jersey.

https://doi.org/10.1124/jpet.117.244855.

ABBREVIATIONS: CL, clearance; FcRn, neonatal Fc receptor; IL, interleukin; ISF, interstitial fluid; LLOQ, lower limit of quantification; mAb, monoclonal antibody; mPBPK, minimal physiologically based pharmacokinetic; PD, pharmacodynamics; PK, pharmacokinetics; PsL, psoriasis-like; rmIL-23, recombinant mouse interleukin-23; TMDD, target-mediated drug disposition.

pharmacological effects (Danhof et al., 2007). These components involved in the exposure-response relationship for biologics often include tissue distribution to the target site, target binding and interaction, and downstream pharmacological cascade. More importantly, mechanism-based models distinguish drug- and system-specific characteristics and provide a way to quantitatively translate the PK/PD relationship between preclinical species and humans (Agoram et al., 2007).

The minimal physiologically based pharmacokinetic (mPBPK) models (Cao and Jusko, 2012; Cao et al., 2013) inherit and lump major physiologic attributes from the whole-body physiologically based pharmacokinetic models and generate physiologically relevant PK parameters, while allowing for assessment of any tissue of interest with the flexibility to add additional tissue compartments. Importantly, with measurements of target interaction in blood or specific tissues of interest, the mPBPK model can incorporate dynamics of target binding and disposition by implementing target-mediated drug disposition (TMDD) kinetics into plasma or the specific tissue compartments (Cao and Jusko, 2014). The first-generation mPBPK model (Cao and Jusko, 2012) is more applicable to small-molecule drugs or small-size proteins. The model includes blood/plasma and one or more lumped tissue compartments. Drug tissue distribution is assumed to be driven by Fick's laws of diffusion. The second-generation mPBPK model is more suitable for biologics such as mAbs (Cao et al., 2013). It adapts all essential components of the full physiologically based pharmacokinetic models for biologics. Tissues are lumped into two compartments (tight or leaky) based on their vascular endothelial structure. Paravascular convection and lymph drainage are assumed to be the dominant pathways for biologics uptake and removal from tissues (Cao et al., 2013).

Our group has previously published work on applying the mPBPK modeling approach to quantitatively assess the kinetics and interrelationship between an anti-IL-6 mAb and IL-6 in both serum and joint lavage fluid in a mouse collagen-induced arthritis model (Chen et al., 2016). A second example focusing on the interplay between an anti-IL-23 mAb and IL-23 in both serum and lesional skin site is presented here.

Repeated intradermal injection of recombinant mouse IL-23 (rmIL-23) into the ear of a mouse induces PsL epidermal hyperplasia, which serves as a suitable preclinical disease model for investigating drug candidates targeting the IL-23/T_h17/IL-17 pathway for psoriatic indications (Kopp et al., 2003; Chan et al., 2006; Rizzo et al., 2011). A mechanistic study was conducted to assess the binding and disposition kinetics of CNTO 3723, a mAb, and its target rmIL-23 in this model. A mPBPK model incorporating TMDD was developed to quantitatively assess the kinetics and interrelationship between CNTO 3723 and rmIL-23 in both serum and lesional skin site. Potential application of this model in translational pharmacology was examined by comparing model predictions to observed ustekinumab effect in psoriatic patients.

Materials and Methods

Test Articles

A rat anti-mouse IL-23 mAb, CNTO 3723, was produced at Janssen R&D, LLC (Spring House, PA) and used in the study. rmIL-23 was purchased from eBioscience (San Diego, CA) and used for development of the IL-23-induced PsL mouse disease model.

Animal Study Design and Sample Collection

The in-life part of the animal study was conducted at WuXi AppTec (Suzhou, China). All studies were approved by the Institutional Animal Care and Use Committee at WuXi AppTec.

CNTO 3723 and rmIL-23 PK Characterization. Healthy C57BL/6 wild-type female mice (n = 52) were randomly assigned to three groups (groups A–C) to study the PK of CNTO 3723 and rmIL-23. Animals in group A (n = 12) received a single intravenous bolus dose of CNTO 3723 at 10 mg/kg. Animals in group B (n = 16) received a single intravenous bolus dose of rmIL-23 at 400 ng. Animals in group C (n = 24) received a single intradermal dose of rmIL-23 at 400 ng into the left ear. Terminal and retro-orbital blood samples were collected at various sampling time points (Table 1).

Target Engagement Assessment in IL-23-Induced PsL Mouse Model. Our previous data had shown that daily intradermal injection of rmIL-23 for five consecutive days can induce PsL inflammation as reflected by ear thickness, ear weight, and histopathology analysis (N. Rozenkrants, internal data). A second set of

TABLE 1
Animal study scheme

Group	Dose		Number of Animals (N)	Sampling Time Point	
	CNTO3723	rmIL-23		Retro-orbital	Terminal
	mg/kg	*ng*			
A	10		12 (4 × 3/each)	15 minutes; 6 hours; 1, 2, 7, and 17 days	2 hours; 2, 14, and 21 days (n = 3/ea)
B		400	16 (4 × 4/each)	15 minutes; 2 and 6 hours; 3 days	1 hour; 1, 2, and 5 days
C		400	24 (6 × 4/each)	30 minutes; 1 and 8 hours; 1 and 3 days	15 minutes; 2 and 6 hours; 1, 2, and 5 days
D	3.3	50	45 (9 × 5/each)	1, 4, and 8 hours after first IL-23 dose; 1 and 8 hours after the fifth IL-23 dose; 5, 8, and 17 days	2 and 24 hours after the first IL-23 dose; 0, 2, 4, and 24 hours after the fifth IL-23 dose; 9, 13, and 22 days
E	3.3	200	45 (9 × 5/each)	1, 4, and 8 hours after first IL-23 dose; 1 and 8 hours after the fifth IL-23 dose; 5, 8, and 17 days	2 and 24 hours after the first IL-23 dose; 0, 2, 4, and 24 hours after the fifth IL-23 dose; 9, 13, and 22 days
F	10	200	45 (9 × 5/each)	1, 4, and 8 hours after first IL-23 dose; 1 and 8 hours after the fifth IL-23 dose; 5, 8, and 17 days	2 and 24 hours after the first IL-23 dose; 0, 2, 4, and 24 hours after the fifth IL-23 dose; 9, 13, and 22 days
G	3.3	500	45 (9 × 5/each)	1, 4, and 8 hours after first IL-23 dose; 1 and 8 hours after the fifth IL-23 dose; 5, 8, and 17 days	2 and 24 hours after the first IL-23 dose; 0, 2, 4, and 24 hours after the fifth IL-23 dose; 9, 13, and 22 days
H	10	200	20 (4 × 5/each)	1 and 24 hours post CNTO 3723 dose on day 0; 0 hours pre- and 24 hours post IL-23 dose on day 2	5 and 15 minutes; 1 and 24 hours post IL-23 dose on day 2

C57BL/6 wild-type female mice ($n = 45 \times 4$) were randomly assigned to four groups (groups D–G) to study CNTO 3723 target engagement in the IL-23-induced PsL mouse disease model. Animals in groups D, E, F, and G received a single intravenous bolus dose of CNTO 3723 at 3.3, 3.3, 10, and 3.3 mg/kg, respectively, on study day 0 and five consecutive daily intradermal injections of rmIL-23 at 50, 200, 200, and 500 ng, respectively, in 10 μl of phosphate-buffered saline/0.1% bovine serum albumin into the lateral left ear on study days 2–6. Another 20 mice in group H were administrated with an intravenous bolus dose of CNTO 3723 at 10 mg/kg on study day 0 and an intradermal injection of 200 ng rmIL-23 into the left ear on study day 2. Terminal and retro-orbital blood samples were collected at various sampling time points (Table 1). At all terminal sampling time points, an 8 mm biopsy punch of each of the two ears were collected from the animal, and tissue homogenate was prepared with Qiagen TissueLyser II (QIAGEN Inc, Germantown, MD) (30 Hz $\times$ 2 minutes) in 500 μl of homogenization buffer containing 1X phosphate-buffered saline with 0.1% bovine serum albumin, 1% Triton X-100, and 2% (v/v) protease inhibitors. The homogenate was centrifuged at 12,000*g* for 15 minutes at 4°C and the collected supernatants was stored at −80°C until analysis.

Bioanalytical Methods

The concentrations of CNTO 3723 in serum and ear tissue homogenates were quantified by a fluorescence-based immunoassay on the GyrolabxP platform (Gyros AB, Uppsala, Sweden). The lower limit of quantification (LLOQ) for both serum and ear tissue homogenate CNTO 3723 concentrations was 80 ng/ml. The concentrations of total and free rmIL-23 in serum and ear tissue homogenates were determined using an electrochemiluminescence-based immunoassay using the Meso Scale Discovery platform (Meso Scale Discovery, Rockville, MD) with a LLOQ of 27.4 pg/ml for both total and free rmIL-23 concentrations in serum and 9.14 pg/ml for both total and free rmIL-23 concentrations in ear tissue homogenates.

A mPBPK Model to Characterize the Interplay between CNTO 3723 and rmIL-23 in IL-23-Induced PsL Mice

The mPBPK model with TMDD features was adapted to characterize the interrelationship between CNTO 3723 and rmIL-23 in IL-23-induced PsL mice. The pharmacokinetics of CNTO 3723 and rmIL-23 in mice were first characterized using second- and first-generation mPBPK models (steps I and II), respectively. Alteration of CNTO 3723 and rmIL-23 pharmacokinetics due to repeated intradermal injections of rmIL-23 into mouse ear were subsequently assessed (step III). Finally, the mPBPK models for rmIL-23 and CNTO 3723 were overlaid with TMDD features incorporated to characterize the interrelationship between CNTO 3723 and rmIL-23 (step IV).

Step I: Serum Pharmacokinetics of CNTO 3723. Serum concentration profiles of CNTO 3723 in animal group A were described with the second-generation mPBPK model. The model includes serum, lymph, and two lumped tissue compartments (leaky and tight, based on vascular endothelium structures) connected in an anatomic manner (Fig. 1A). The model is described as follows:

$$\frac{dC_s}{dt} = \frac{C_{lymph} \cdot L - C_s \cdot L_1 \cdot (1-\sigma_1) - C_s \cdot L_2 \cdot (1-\sigma_2) - C_s \cdot CL_s}{V_s},$$

$$C_s(0) = \frac{Dose}{V_s} \quad (1)$$

$$\frac{dC_{tight}}{dt} = \frac{C_s \cdot L_1 \cdot (1-\sigma_1) - L_1 \cdot (1-\sigma_L) \cdot C_{tight}}{V_{tight}},\ C_{tight}(0) = 0 \quad (2)$$

$$\frac{dC_{leaky}}{dt} = \frac{C_s \cdot L_2 \cdot (1-\sigma_2) - L_2 \cdot (1-\sigma_L) \cdot C_{leaky}}{V_{leaky}},\ C_{leaky}(0) = 0 \quad (3)$$

$$\frac{dC_{lymph}}{dt} = \frac{L_1 \cdot (1-\sigma_L) \cdot C_{tight} + L_2 \cdot (1-\sigma_L) \cdot C_{leaky} - C_{lymph} \cdot L}{V_{lymph}},$$

$$C_{lymph}(0) = 0 \quad (4)$$

where C_s, C_{tight}, and C_{leaky} are the concentrations of CNTO 3723 in serum and interstitial fluid (ISF) in two types of lumped tissues

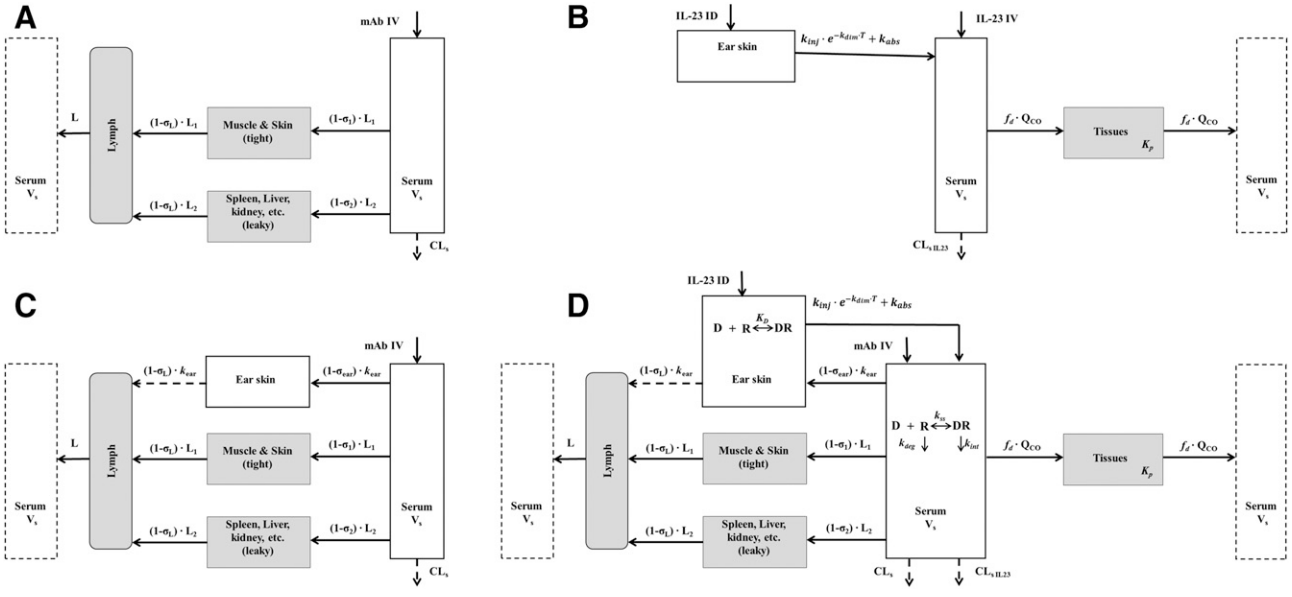

Fig. 1. Scheme of mPBPK models with TMDD features developed stepwise for characterization of distribution of CNTO 3723 and its interrelationship with rmIL-23 in serum and ear skin in IL-23-induced PsL mice. (A) Second-generation mPBPK model applied for the characterization of serum pharmacokinetics of CNTO 3723 in step I. (B) First-generation mPBPK model applied for the characterization pharmacokinetics of rmIL-23 in step II. (C) Second-generation mPBPK model including ear skin tissue compartment for the characterization of distribution of CNTO 3723 to ear skin in step III. (D) First- and second-generation mPBPK models overlaid with TMDD features incorporated in serum and ear skin compartments for the characterization of the interplay between CNTO 3723 and rmIL-23 in step IV.

categorized by continuous and fenestrated vascular endothelium, and C_{lymph} is the concentration of CNTO 3723 in lymph; V_{tight} (0.65 · ISF · K_p, where K_p is the available fraction of ISF for antibody distribution) and V_{leaky} (0.35 · ISF · K_p) are the ISF volumes of the two lumped tissues (Cao et al., 2013); V_{lymph} represents the lymph volume, which is assumed equal to the blood volume; L is the total lymph flow rate, in which L_1 and L_2 account for one-third and two-thirds of the total lymph flow (Cao et al., 2013); σ_1 and σ_2 are the vascular reflection coefficients for leaky and tight tissues; σ_L is the lymphatic capillary reflection coefficient and is assumed to be 0.2 (Cao et al., 2013); and CL_s represents the linear serum clearance of CNTO 3723.

Step II: Pharmacokinetics of rmIL-23. The serum and ear homogenate concentration profiles of rmIL-23 in animal groups B and C were fitted with a first-generation mPBPK model to characterize the pharmacokinetics of rmIL-23. The model has a serum compartment and lumps all tissues into one tissue compartment (Fig. 1B). Following intravenous bolus administration, the model is described as follows:

$$\frac{dC_{\text{s IL23}}}{dt} = \frac{-C_{\text{s IL23}} \cdot (CL_{\text{s IL23}} + f_d \cdot Q_{CO}) + (C_{\text{t IL23}}/K_p) \cdot f_d \cdot Q_{CO}}{V_s}, \quad C_{\text{s IL23}}(0) = \frac{\text{Dose}}{V_s} \tag{5}$$

$$\frac{dC_{\text{t IL23}}}{dt} = \frac{C_{\text{s IL23}} \cdot f_d \cdot Q_{CO} - (C_{\text{t IL23}}/K_p) \cdot f_d \cdot Q_{CO}}{V_t}, \; C_{\text{t IL23}}(0) = 0 \tag{6}$$

where $C_{\text{s IL23}}$ and $C_{\text{t IL23}}$ are the concentrations of rmIL-23 in serum (V_s) and tissue ISF (V_t); Q_{CO} is the cardiac plasma flow (Cao and Jusko, 2012); f_d is the fraction of Q_{CO} for V_t; K_p is the tissue partition coefficient; and $CL_{\text{s IL23}}$ is the serum clearance.

The absorption kinetics following intradermal injection of rmIL-23 in the ear was assumed to be mixed exponential-decay and constant first-order absorption kinetics. Following intradermal injection in the ear, the model is described as follows:

$$\frac{dA_{\text{ear IL23}}}{dt} = -\left(k_{\text{inj}} \cdot e^{-k_{\text{dim}} \cdot t} + k_{\text{abs}}\right) \cdot A_{\text{ear}}, \; A_{\text{ear}}(0) = \text{Dose} \tag{7}$$

$$\frac{dC_{\text{s IL23}}}{dt} = \frac{(k_{\text{inj}} \cdot e^{-k_{\text{dim}} \cdot t} + k_{\text{abs}}) \cdot F \cdot A_{\text{ear IL-23}} - C_{\text{s IL23}} \cdot (CL_{\text{s IL23}} + f_d \cdot Q_{CO}) + (C_{\text{t IL23}}/K_p) \cdot f_d \cdot Q_{CO}}{V_s}, \quad C_{\text{s IL23}}(0) = 0 \tag{8}$$

$$\frac{dC_{\text{t IL23}}}{dt} = \frac{C_{\text{s IL23}} \cdot f_d \cdot Q_{CO} - (C_{\text{t IL23}}/K_p) \cdot f_d \cdot Q_{CO}}{V_t}, \; C_{\text{t IL23}}(0) = 0 \tag{9}$$

where A_{ear} is the amount of rmIL-23 at the site of injection; k_{inj} is the first-order absorption rate constant caused by blister formation following intradermal injection; k_{dim} is the exponential decay factor used to describe the blister healing process; k_{abs} is the first-order absorption rate constant from the dermis; and F represents bioavailability. The remaining symbols are the same as previously defined.

The measured concentration of rmIL-23 in ear homogenates is described as follows:

$$C_{\text{ear IL23}} = \frac{A_{\text{ear IL23}}}{V_{\text{buffer}}} \times \alpha_{\text{rec}} \tag{10}$$

where V_{buffer} is the volume of buffer used to prepare the ear tissue homogenate (V_{buffer} = 0.5 ml), and α_{rec} is the recovery rate of rmIL-23 following tissue sampling and homogenate procedures (α_{rec} = 10%).

Step III: Impact of Repeated Intradermal Injection of rmIL-23 on the Pharmacokinetics of rmIL-23 and CNTO 3723. Our data showed that repeated intradermal injections of rmIL-23 in mouse ear led to alteration in the pharmacokinetics for both rmIL-23 and CNTO 3723 (see Fig. 3 for details).

Impact on rmIL-23 absorption. Following repeated rmIL-23 administration, the apparent decrease in the rate of absorption of rmIL-23 from ear following each additional dose was described by a decrease in the first-order absorption rate constant (k_{abs}). The concentration profiles of total rmIL-23 in ear homogenates in groups D–H were applied to fit with the absorption kinetics model (eq. 7). Parameters related to rmIL-23 intradermal absorption estimated previously (see *Step II: Pharmacokinetics of rmIL-23*) were fixed. To account for the alteration in rmIL-23 absorption kinetics k_{abs}, following the nth dose, is described as follows:

$$k_{\text{abs\_}N} = k_{\text{abs}} \cdot \left[1 - (N_{\text{ID}} - 1) \cdot \text{fac}_{\text{lym}}\right] \tag{11}$$

where N_{ID} represents the nth rmIL-23 intradermal injection, and fac_{lym} is the ratio decrease in k_{abs} following each rmIL-23 intradermal dose. The remaining symbols are the same as previously defined.

Impact on CNTO 3723 disposition. Upon intradermal injection of rmIL-23 into mouse ear, the CNTO 3723 concentration profiles in ear homogenates exhibited an apparently enhanced and oscillated tissue distribution. The distribution kinetics values of CNTO 3723 in mouse ear skin were characterized by incorporating an ear skin compartment into the second-generation mPBPK model (Fig. 1C). CNTO 3723 concentration profiles in serum and ear homogenates in healthy control and IL-23-induced PsL mice (groups A and D–H) were examined. Parameters related to CNTO 3723 serum pharmacokinetics estimated previously (see *Step I: Serum Pharmacokinetics of CNTO 3723*) were fixed. Together with eqs. 1–5 the model addition is as follows:

$$\frac{dC_{\text{ear ISF}}}{dt} = \frac{C_s \cdot V_{\text{ear ISF}} \cdot k_{\text{ear}} \cdot (1 - \sigma_{\text{ear}}) - C_{\text{ear ISF}} \cdot V_{\text{ear ISF}} \cdot k_{\text{ear}} \cdot \left(1 - \text{scal} \cdot e^{-d_{\text{lym}} \cdot T_{\text{post IL23}}}\right) \cdot (1 - \sigma_L)}{V_{\text{ear ISF}}}, \quad C_{\text{ear ISF}}(0) = 0 \tag{12}$$

where $C_{\text{ear ISF}}$ represents the CNTO 3723 concentration in mouse ear ISF space ($V_{\text{ear ISF}}$); k_{ear} is the ear ISF turnover rate and is represented as the lymph flow rate (L_{ear}) divided by $V_{\text{ear ISF}}$; and σ_{ear} is the vascular reflection coefficient for mouse ear skin. The remaining symbols are the same as previously defined. The quantity of CNTO 3723 in mouse ear biopsy puncture was minimal compared to that in systemic circulation. Therefore, the impact of CNTO 3723 outflow from mouse ear on serum CNTO 3723 was not included.

For healthy control mice before rmIL-23 injection

$$\sigma_{\text{ear}} = \sigma_{\text{ear ctrl}} \tag{13a}$$

For IL-23-induced PsL mice (mice after rmIL-23 injection on day 2)

$$\sigma_{\text{ear}} = \sigma_{\text{ear PsL}} \tag{13b}$$

Immediately following each rmIL-23 treatment, the CNTO 3723 concentration in ear homogenates exhibited a transient increase and then decreased as CNTO 3723 was eliminated from serum (Fig. 3A). The term $(1 - \text{scal} \cdot e^{-d\text{lym} \cdot T\text{post IL23}})$ is applied to account for the oscillation of CNTO 3723 concentration profiles in ear homogenates following intradermal injection of rmIL-23, where scal is the maximum decrease in the ear skin lymph flow rate immediately following each rmIL-23 intradermal injection, d_{lym} is the exponential rate constant of remission of lymph propulsion, and $T_{\text{post IL23}}$ represents the time post rmIL-23 administration.

The measured concentration of CNTO 3723 in ear homogenates is described as follows:

$$C_{\text{ear}} = \frac{C_{\text{ear ISF}} \cdot V_{\text{ear ISF}} + C_s \cdot V_{\text{ear Vas}}}{V_{\text{buffer}}} \tag{14}$$

where $V_{\text{ear ISF}}$ and $V_{\text{ear Vas}}$ are the volume of ISF and residual vascular space, respectively, of the ear skin biopsy sample (W_{ear}). For mice in

the healthy control group (group A) and mice in the rmIL-23 treatment groups (groups D–H) prior to day 2, W_{ear} was on average of 10 mg. Upon rmIL-23 administration post day 2 in groups D–H, ear weight and thickness increased, and W_{ear} was on average 15 mg. The ISF and residual vascular spaces accounted for 15% and 5% of the total tissue volume, assuming 1 g is equal to 1 ml. The remaining symbols are the same as previously defined.

Step IV: Interrelationship between CNTO 3723 and rmIL-23. The interrelationship between CNTO 3723 and rmIL-23 was assessed by overlaying the first- and second-generation mPBPK models with the TMDD features incorporated (Fig. 1D). CNTO 3723 and free and total rmIL-23 concentration profiles in serum and ear homogenates in groups D–H were applied to simultaneously fit with the model. Free rmIL-23 concentrations in serum were below the LLOQ at all time points and were not used for model development. Parameters that have been estimated from previous steps were fixed. The model assumed that rmIL-23 and CNTO 3723 binding in ear tissue homogenates reached equilibrium and had the binding dissociation constant (K_D) estimated. The model is described as follows:

$$\frac{dC_s}{dt} = \frac{C_{lymph} \cdot L - C_{free} \cdot L_1 \cdot (1-\sigma_1) - C_{free} \cdot L_2 \cdot (1-\sigma_2) - C_{free} \cdot CL_s}{V_s} - AR \cdot k_{int},\ C_s(0) = \frac{Dose}{V_p} \tag{15}$$

$$\frac{dC_{tight}}{dt} = \frac{C_{free} \cdot L_1 \cdot (1-\sigma_1) - L_1 \cdot (1-\sigma_L) \cdot C_{tight}}{V_{tight}},\ C_{tight}(0) = 0 \tag{16}$$

$$\frac{dC_{leaky}}{dt} = \frac{C_{free} \cdot L_2 \cdot (1-\sigma_2) - L_2 \cdot (1-\sigma_L) \cdot C_{leaky}}{V_{leaky}},\ C_{leaky}(0) = 0 \tag{17}$$

$$\frac{dC_{lymph}}{dt} = \frac{L_1 \cdot (1-\sigma_L) \cdot C_{tight} + L_2 \cdot (1-\sigma_L) \cdot C_{leaky} - C_{lymph} \cdot L}{V_{lymph}},\ C_{lymph}(0) = 0 \tag{18}$$

$$\frac{dC_{ear\ ISF}}{dt} = \frac{C_{free} \cdot V_{ear\ ISF} \cdot k_{ear} \cdot (1-\sigma_{ear}) - C_{ear\ ISF} \cdot V_{ear\ ISF} \cdot k_{ear} \cdot \left(1 - scal \cdot e^{-d_{lym} \cdot T_{post\ IL23}}\right) \cdot (1-\sigma_L)}{V_{ear\ ISF}},\ C_{ear\ ISF}(0) = 0 \tag{19}$$

$$\frac{dA_{ear\ IL23}}{dt} = -\left(k_{inj} \cdot e^{-k_{dim} \cdot t} + k_{abs}\right) \cdot A_{ear\ IL23},\ A_{ear}(0) = \text{Dose} \tag{20}$$

$$\frac{dC_{s\ IL23}}{dt} = \frac{\left(k_{inj} \cdot e^{-k_{dim} \cdot t} + k_{abs}\right) \cdot F \cdot A_{ear\ IL23} \cdot 0.05 - (C_{s\ IL23} - AR) \cdot CL_{s\ IL23} - C_{s\ IL23} \cdot f_d \cdot Q_{CO} + \left(C_{t\ IL23}/K_p\right) \cdot f_d \cdot Q_{CO}}{V_s} - AR \cdot k_{int},\ C_{s\ IL23}(0) = 0 \tag{21}$$

$$\frac{dC_{t\ IL23}}{dt} = \frac{C_{s\ IL23} \cdot f_d \cdot Q_{CO} - \left(C_{t\ IL23}/K_p\right) \cdot f_d \cdot Q_{CO}}{V_t},\ C_{t\ IL23}(0) = 0 \tag{22}$$

where C_{free} is the free CNTO 3723 concentration in serum; $C_{s\ IL23}$ is the total rmIL-23 concentration in serum; AR is the CNTO 3723-rmIL-23 complex concentration in serum; and k_{int} is the elimination rate constant of the CNTO 3723-rmIL-23 complex in serum. The remaining symbols are the same as previously described. In addition, in eq. 21, an arbitrary factor of 0.05 was applied to adjust the absorption of rmIL-23 in serum from intradermal injection in ear based on the observed serum level of rmIL-23.

Assuming quasi-equilibrium condition, the free CNTO 3723 concentration in serum (C_{free}) can be described as follows (Gibiansky et al., 2008):

$$C_{free} = \frac{(C_s - K_{ss} - C_{s\ IL23}) - \sqrt{(C_s - K_{ss} - C_{s\ IL23})^2 + 4 \cdot C_s \cdot K_{ss}}}{2} \tag{23}$$

The K_{ss} value is the steady-state constant defined as follows:

$$K_{ss} = \frac{k_{int} + k_{off}}{k_{on}} \tag{24}$$

where the k_{on} and k_{off} refer to the CNTO 3723-IL-23 association and dissociation rate constants, respectively; and AR can be described as follows:

$$AR = C_{s\ IL23} \cdot \frac{C_{free}}{K_{ss} + C_{free}} \tag{25}$$

Assuming rmIL-23 and CNTO 3723 in ear tissue homogenates reached binding equilibrium, the free concentration of CNTO 3723 in ear homogenate ($C_{free\ EH}$) is described as follows (Gibiansky et al., 2008):

$$C_{free\ EH} = \frac{(C_{ear} - K_D - C_{ear\ IL23}) - \sqrt{(C_{ear} - K_D - C_{ear\ IL23})^2 + 4 \cdot C_{ear} \cdot K_D}}{2} \tag{26}$$

where C_{ear} and $C_{ear\ IL23}$ are the measured concentrations of total CNTO 3723 and rmIL-23 in ear tissue homogenates previously defined in eqs. 14 and 10; and K_D is the binding dissociation coefficient (k_{off}/k_{on}). The free rmIL-23 concentration in ear homogenates is

$$C_{ear\ fIL23} = C_{ear\ IL23} \cdot \frac{K_D}{K_D + C_{free\ EH}} \tag{27}$$

Prediction of Ustekinumab Effect in Humans

To evaluate the translational utility of the developed preclinical mechanism-based mPBPK model, the mPBPK model results and the ustekinumab human PK and psoriatic patient disease pathophysiology information were integrated to predict ustekinumab effect in psoriatic patients. The integrated information included: 1) CNTO 3723 tissue distribution kinetics and interaction with rmIL-23 in serum and lesional skin sites in IL-23-induced PsL mice, in which these parameters were assumed to be the same in psoriatic patients; 2) serum ustekinumab pharmacokinetics in psoriatic patients (Zhu et al., 2010); 3) ustekinumab binding affinity with human IL-23 (internal data); and 4) IL-23 baseline concentrations in healthy and psoriatic patients (El Hadidi et al., 2008). The model structure for translational PK/PD application is shown in Fig. 2. The model includes only the central compartment and the lesional skin compartment. Serum concentration of ustekinumab in psoriatic patients was used as the driving function for its distribution and exposure in lesional skin sites (Fig. 2, dashed lines and arrows). The tissue distribution kinetics is governed by the lymph flow turnover rate of skin (k_{skin}) and vascular permeability (σ_{skin}). TMDD features were incorporated in both serum and lesional skin compartments for characterization of the interaction of ustekinumab with IL-23. The model is described as follows:

$$\frac{dC_{s\ mAb}}{dt} = \frac{input - C_{s\ fmAb} \cdot CL - k_{s\ int} \cdot AR_s \cdot V}{V},\ C_{s\ mAb}(0) = 0 \tag{28}$$

$$\frac{dC_{t\ mAb}}{dt} = C_{s\ fmAb} \cdot k_{skin} \cdot (1-\sigma_{skin}) - C_{t\ fmAb} \cdot k_{skin} \cdot (1-\sigma_L) - AR_t \cdot k_{t\ int},\ C_{t\ mAb}(0) = 0 \tag{29}$$

$$\frac{dC_{s\ IL23}}{dt} = k_{s\ syn} - k_{s\ deg} \cdot (C_{s\ IL23} - AR_s) - AR_s \cdot k_{s\ int},\ C_{s\ IL23}(0) = C_{s\ IL23b} \tag{30}$$

$$\frac{dC_{t\ IL23}}{dt} = k_{t\ syn} - k_{t\ deg} \cdot (C_{t\ IL23} - AR_t) - AR_t \cdot k_{t\ int},\ C_{s\ IL23}(0) = C_{t\ IL23b} \tag{31}$$

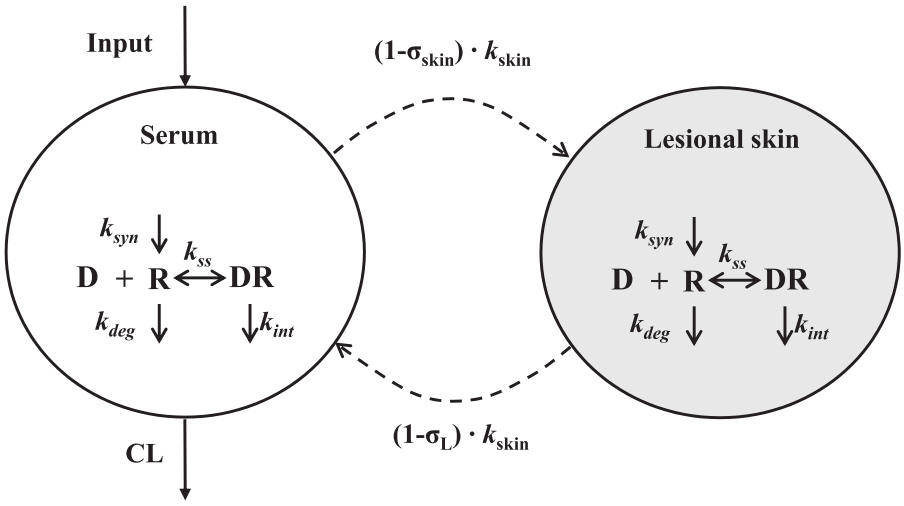

Fig. 2. Scheme of translational PK/PD model applied for ustekinumab pharmacological effect prediction in psoriatic patients.

where $C_{s\ mAb}$, $C_{t\ mAb}$, $C_{s\ IL23}$, and $C_{t\ IL23}$ are the total concentrations of ustekinumab and IL-23 concentration in serum and lesional skin ISF; $C_{s\ fmAb}$ and $C_{t\ fmAb}$ are free ustekinumab concentrations in serum and lesional skin ISF, respectively; AR_s and AR_t are the ustekinumab-IL-23 complex concentrations in serum and lesional skin ISF, respectively; CL and V are the clearance and volume of ustekinumab of the central compartment, respectively; $k_{s\ int}$ and $k_{t\ int}$ are the serum and skin tissue elimination rate constants of AR_s and AR_t, respectively; $k_{s\ syn}$, $k_{s\ deg}$, $k_{t\ syn}$, and $k_{t\ deg}$ are the synthesis and degradation rate constants of IL-23 in serum and skin ISF; and $C_{s\ IL23b}$ and $C_{t\ IL23b}$ represent the baseline concentrations of IL-23 in psoriatic patients.

Assuming quasi-equilibrium condition, $C_{s\ fmAb}$ and $C_{t\ fmAb}$ can each be described as follows (Gibiansky et al., 2008):

$$C_{s\ fmAb} = \frac{(C_{s\ mAb} - K_{s\ ss} - C_{s\ IL23}) - \sqrt{(C_{s\ mAb} - K_{s\ ss} - C_{s\ IL23})^2 + 4 \cdot C_{s\ mAb} \cdot K_{s\ ss}}}{2} \quad (32)$$

$$C_{t\ fmAb} = \frac{(C_{t\ mAb} - K_{t\ ss} - C_{t\ IL23}) - \sqrt{(C_{t\ mAb} - K_{t\ ss} - C_{t\ IL23})^2 + 4 \cdot C_{t\ mAb} \cdot K_{t\ ss}}}{2} \quad (33)$$

where $K_{s\ ss}$ and $K_{t\ ss}$ are the steady-state constants in serum and skin ISF, respectively, and are defined as follows:

$$K_{s\ ss} = \frac{k_{s\ int} + k_{off}}{k_{on}} \quad (34)$$

$$K_{t\ ss} = \frac{k_{t\ int} + k_{off}}{k_{on}} \quad (35)$$

where k_{on} and k_{off} refer to the ustekinumab association and dissociation rate constants, respectively, against IL-23; and AR_s and AR_t can be described as follows:

$$AR_s = C_{s\ IL23} \cdot \frac{C_{s\ fmAb}}{K_{s\ ss} + C_{s\ fmAb}} \quad (36)$$

$$AR_t = C_{t\ IL23} \cdot \frac{C_{t\ fmAb}}{K_{t\ ss} + C_{t\ fmAb}} \quad (37)$$

Model Fitting and Analysis

Model fittings and simulations were performed using NONMEM version 7.2 (ICON Development Solutions, Ellicott City, MD), and the naive pooling approach was used for model fitting since the data were from serial destruction and were being pooled together. Between-subject variability (IIV) was not considered and the omega matrix was fixed to zero. The first-order method was used. The variance model used is

$$V_i = (\sigma_a + \sigma_p \cdot Y_i)^2 \quad (38)$$

where V_i is the variance of the ith observation; σ_a and σ_p are the additive and proportional variance model parameters, respectively; and Y_i is the ith model prediction. Measurements below the LLOQ were treated as missing values. Model performance was evaluated by goodness-of-fit plots and objective function values. GraphPad Prism (GraphPad Software Inc., San Diego, CA) was used to produce the graphs.

Results

Serum Pharmacokinetics of CNTO 3723 (Step I)

Following 10 mg/kg i.v. administration, the concentration profile of CNTO 3723 in serum in healthy mice showed a biexponential feature with a slow terminal elimination phase (Fig. 4, group A, symbols). The pharmacokinetics of CNTO 3723 in normal mice in the absence of any exogenous rmIL-23 dosing was first characterized with a second-generation mPBPK model. Noncompartmental analysis showed that CNTO 3723 exhibited approximately linear pharmacokinetics between the 3.3 and 10 mg/kg dose range, and this is consistent with the expectation for a mAb that binds to a low-abundance soluble ligand. Model-fitted serum concentrations of CNTO 3723 were overlaid with the observed concentrations in healthy mice (Fig. 4, group A). The parameter estimates and the relative S.E. values are listed in Table 2. Overall, the model was able to characterize the serum concentration profiles of CNTO 3723 reasonably well. The estimated linear clearance of CNTO 3723 translates to a serum half-life of about 8 days, which is consistent with the reported serum half-life of typical murine IgG levels in mice (Vieira and Rajewsky, 1988). The vascular reflection coefficient for tight tissue (σ_1) was fixed at 0.98 to obtain precise parameter estimates (Cao and Jusko, 2014). The estimated vascular reflection coefficient for leaky tissue (σ_2) was 0.657, suggesting moderate tissue distribution.

Pharmacokinetics of rmIL-23 (Step II)

The concentration profiles of rmIL-23 in serum following single intravenous administration in mice (Fig. 7, group B, symbols) showed that rmIL-23 is cleared from serum rapidly (below the LLOQ within 1 hour). However, following intradermal

TABLE 2
Summary of model parameters and estimates

Parameter	Definition	Estimate	Relative S.E.
			%
Step I: PK of CNTO 3723			
σ_1	Vascular reflection coefficient of tight tissue	0.98	Fixed
σ_2	Vascular reflection coefficient of leaky tissue	0.657	8
CL_{ctrl} (ml/day)	Linear serum clearance	0.0708	14
Step II: PK of rmIL-23			
f_d	Fraction of Q_{CO} for V_t	0.0023	10
K_p	Partition coefficient	1	Fixed
$CL_{s\ IL23}$ (ml/day)	Linear serum clearance	307	8
F	Bioavailability	0.0164	11
k_{abs} (1/day)	Regular intradermal absorption rate constant	1.88	38
k_{inj} (1/day)	Absorption rate constant from intradermal caused by blister formation	53.6	19
k_{dim} (1/day)	Rate constant of blister healing process	12.3	31
Step III: PK alteration of rmIL-23 and CNTO 3723 (alteration of rmIL-23 PK)			
fac_{lym}	Ratio decrease in k_{abs} following each rmIL-23 intradermal dose	0.224	7
Step III: PK alteration of rmIL-23 and CNTO 3723 (alteration of CNTO 3723 PK)			
σ_{ear_ctrl}	Vascular reflection coefficient of ear in healthy mice	0.925	1
σ_{ear_PsL}	Vascular reflection coefficient of ear in PsL mice	0.723	9
k_{ear} (1/day)	Ear lymph flow turnover rate	13	38
scal	Maximum ratio decrease in lymph flow rate	0.9	Fixed
d_{lym} (1/day)	Remission rate of lymph propulsion	1.19	12
Step IV: Interrelationship between CNTO 3723 and rmIL-23			
K_D (nM)	Binding dissociation coefficient	0.12	55
k_{int} (1/day)	Elimination rate constant of complex in serum	0.65	24
Physiologic parameters of mouse (25 g)			
V_s (ml)[a]	Serum volume	0.85	
ISF (ml)[a]	Total tissue interstitial space volume	4.35	
V_{lymph} (ml)[a]	Lymph volume	1.53	
L (ml/day)[b]	Total lymph flow rate	2.88	
Q_{CO} (ml/day)[c]	Cardiac plasma flow rate	20,950	

[a]Physiologic parameter values obtained from Shah and Betts (2012); assumed 25 g body weight.
[b]Total lymphatic flow allometrically scaled from human (2.9 l/day) with exponent factor 0.74.
[c]Physiologic parameter values obtained from Shah and Betts (2012); assumed 25 g body weight.

injection in the ear, the serum concentration profile of rmIL-23 showed a shallower slope (Fig. 7, group C, symbols), suggesting flip-flop pharmacokinetics, i.e., longer apparent half-life due to the slower absorption process.

A first-generation mPBPK model was developed to describe the rmIL-23 pharmacokinetics. Following intradermal injection, the disappearance of rmIL-23 in ear homogenates was biphasic (Fig. 6, group C, symbols). Given the low serum levels of rmIL-23, the biphasic profile of rmIL-23 in ear homogenate was most likely due to absorption from the injection site, rather than tissue distribution from central circulation. One possible physiologic explanation for the observed time-dependent absorption kinetics is that the absorption kinetics is composed of a first-order regular intradermal absorption process and an initially faster absorption process, e.g., driven by increased hydrostatic pressure due to blister formation, and this faster absorption process is gradually dampened as the blister heals. The model-fitted concentration profiles of rmIL-23 in serum and ear homogenates and parameter estimates are listed in Figs. 6 and 7 (groups B and C) and Table 2. The observed concentration profiles of rmIL-23 were well captured with this proposed parallel absorption model. The model-estimated serum clearance of rmIL-23 was 307 day^{-1}, indicating rapid serum elimination (half-life of about 3 minutes). The estimated fraction of cardiac plasma flow (Q_{CO}) for tissue ISF space (f_d) was 0.002, suggesting that rmIL-23 tissue distribution is diffusion-rate limited. Given the size of rmIL-23 and its hydrophilic property, it cannot readily exchange and equilibrate out between serum and tissue ISF. The partition coefficient (K_p) was estimated to be close to 1 during model fitting and subsequently fixed to 1, suggesting that the entire space of tissue ISF is available for rmIL-23 distribution. Following ear intradermal injection, the bioavailability (F) was low (0.0164), suggesting poor intradermal bioavailability. The estimated regular intradermal absorption rate constant (k_{abs}) was 1.88 day^{-1}, which is closed to the skin lymph turnover rate (0.69 day^{-1} in human and 5.31 day^{-1} in mice when allometrically scaled with the exponent −0.25) (Ibrahim et al., 2012). This indicates that regular intradermal absorption of rmIL-23 into circulation is likely governed by the lymph flow. The first-order absorption rate constant associated with blister formation (k_{inj}) following intradermal injection was 53.6 day^{-1}, which was ~30-fold higher than k_{abs}. The rate constant of the blister healing process (k_{dim}) was 12.3 day^{-1}, which suggests that the blister heals in 4–6 hours.

Impact of Repeated Intradermal Injections of rmIL-23 on the Pharmacokinetics of CNTO 3723 and rmIL-23 (Step III)

To investigate the interaction between CNTO 3723 and rmIL-23 under PsL conditions, five repeated daily intradermal injections of rmIL-23 were given in mouse ear. PsL

inflammation was confirmed via ear thickness, ear weight, and histopathology analysis (data not shown). Interestingly, with the daily intradermal injection of rmIL-23, alterations of concentration profiles of CNTO 3723 and rmIL-23 in ear homogenates were observed, which were possibly due to pathophysiological changes upon repeated rmIL-23 administration.

Impact on CNTO 3723 Disposition. Repeated intradermal injections of rmIL-23 did not alter the systemic clearance of CNTO 3723. However, enhanced tissue uptake of CNTO 3723 into ear has been observed following administration of rmIL-23. Importantly, the concentration of CNTO 3723 exhibited transient increase immediately following each rmIL-23 intradermal administration (Fig. 3A). We hypothesized that the enhanced and oscillated tissue distribution of CNTO 3723 in ear could be attributed to the increased vascular permeability and temporary cessation of lymph propulsion following rmIL-23 intradermal administration. This is supported by the report that intradermal injection of inflammatory cytokines could interfere with lymph propulsion at the injection site in mice, possibly mediated via the nitric oxide pathway (Aldrich and Sevick-Muraca, 2013). The mPBPK model was modified accordingly based on this hypothesis (see *Materials and Methods*). The concentration profiles of CNTO 3723 in serum and ear homogenates were well characterized by the proposed model (Figs. 4 and 5). The estimated vascular reflection coefficients for ear skin (σ_{ear}) were 0.925 and 0.723 for healthy and PsL mice, respectively, suggesting increased vascular permeability in PsL mice compared with healthy control mice. At steady state, CNTO 3723 concentrations in ear skin ISF were around 10% and 25% of serum concentration in healthy and PsL mice, respectively, which are mostly consistent with the extent of tissue distribution of secukinumab in healthy subjects and psoriatic patients (23% and 28%, respectively) as determined by dermal open-flow microperfusion (Dragatin et al., 2016), and slightly lower than the reported skin ISF exposure for an anti-IL-17 IgG (~50%) by tissue centrifugation (Eigenmann et al., 2017). The estimated ear skin lymph turnover rate was 13 day^{-1}, which corresponds with previously measured skin lymph turnover rates (Ibrahim et al., 2012). The maximum decrease of lymph flow rate (scal) was estimated to be close to 1 and subsequently fixed to 0.9. The estimated lymph propulsion remission rate (d_{lym}) was 1.19 day^{-1}. Following each intradermal injection of rmIL-23, the tissue elimination rate of CNTO 3723 via lymph flow was immediately dropped to 10% and gradually recovered to 80% after 24 hours.

Impact on rmIL-23 Absorption. Following repeated rmIL-23 intradermal administration, an apparent slower absorption of rmIL-23 from ear was observed following the fifth dose compared with the first dose, i.e., the amount of rmIL-23 remained at the injection site 24 hours after dosing and was considerably higher following the fifth dose than that following the first dose (Fig. 3B). One possible explanation is that the local lymph flow was damaged following repeated intradermal injections of rmIL-23. No sample was taken following the second, third, or fourth dose, but it is reasonable to assume that this potential impact on local lymph flow is gradual. The mPBPK model was modified accordingly to reflect the change in the rmIL-23 absorption process (see *Materials and Methods*). The change in intradermal absorption kinetics of rmIL-23 seemed to be more relevant to the repeated intradermal injection handling than the actual dose level of rmIL-23. In addition, the comparison of rmIL-23

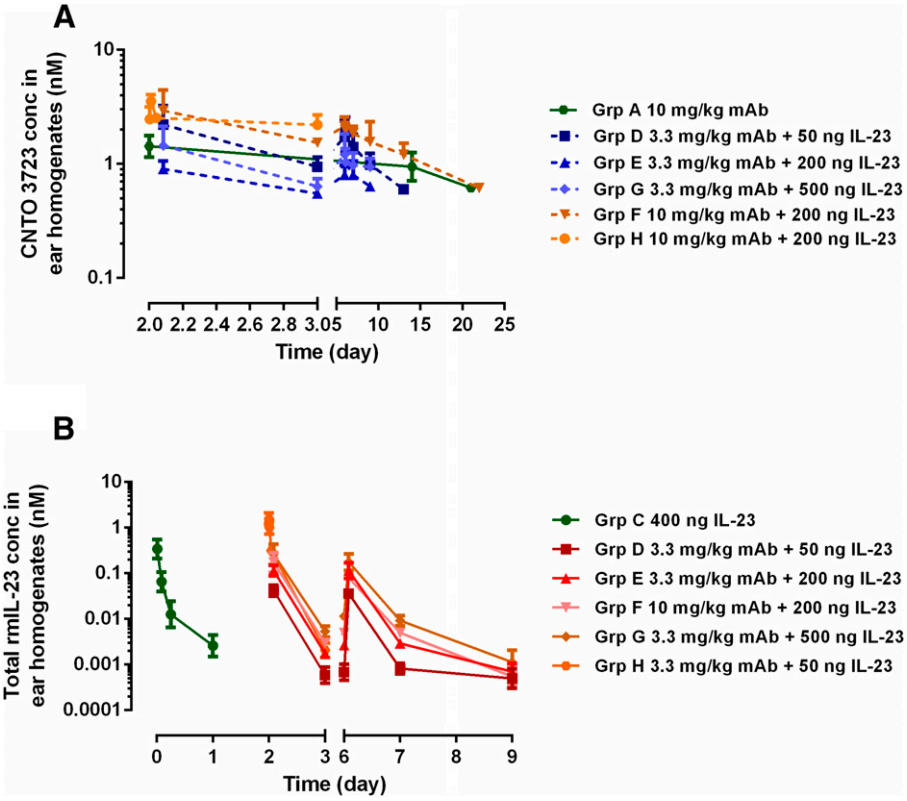

Fig. 3. Alterations of concentration profiles CNTO 3723 and rmIL-23 in ear homogenates following repeated IL-23 intradermal treatment. (A) CNTO 3723 concentration profiles in ear homogenates in all treatment groups. Compared with nontreated animals (group A), at the same CNTO3723 doses, enhanced CNTO 3723 ear distribution was observed following intradermal treatment with rmIL-23 (groups F and H). Also, immediately following rmIL-23 intradermal treatment, the ear concentration of CNTO3723 showed transient increase when comparing CNTO 3723 concentration at day 3 (right before the second rmIL-23 dose) and day 6 (immediately after the fifth rmIL-23 dose). (B) rmIL-23 concentration profiles in ear homogenates in all treatment groups. The concentration profiles following the first rmIL-23 intradermal dose with concurrent CNTO 3723 treatment in groups D–H showed similar kinetics with that following rmIL-23 treatment alone (group C). Also, following the fifth intradermal dose (days 6 and 7), rmIL-23 showed slower clearance in ear compared with that following the first dose (days 2 and 3).

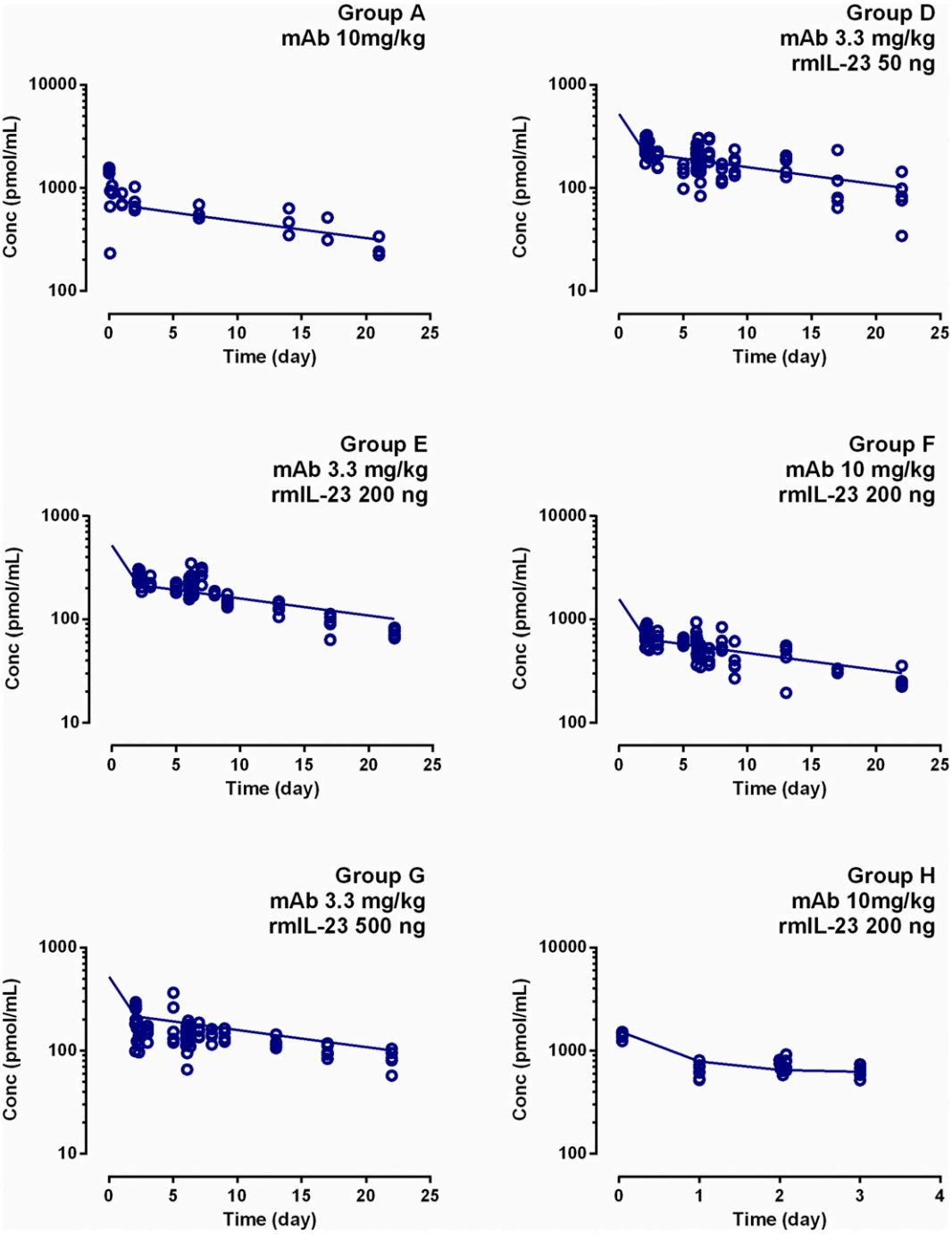

Fig. 4. Model-fitted serum CNTO 3723 concentrations vs. time profiles. Circles are measured concentrations and curves depict model fittings.

concentration profiles in ear homogenates between group C (without CNTO 3723 dosing) and groups D–H (with CNTO 3723 dosing) following the first rmIL-23 administration showed no apparent change in the rmIL-23 absorption kinetics, indicating that the presence of CNTO 3723 did not change the absorption of rmIL-23 (Fig. 3B). The model-fitted concentration profiles of total rmIL-23 in ear homogenates across all animal groups are shown in Fig. 6, groups D–H. In general, the observed data were well characterized using the proposed model. The estimated ratio decrease in k_{abs} following each injection was 0.224, suggesting that the lymph uptake-mediated absorption decreases 22% after each additional injection.

Interrelationship between CNTO 3723 and rmIL-23 (Step IV)

Finally, the interrelationship between CNTO 3723 and rmIL-23 was characterized by overlaying the two mPBPK models for both components and including the TMDD features in serum and ear skin compartments. Free rmIL-23 concentration profiles in ear homogenates and total rmIL-23 concentration profiles in serum were all applied simultaneously for model fitting. The model-fitted concentration profiles of all components well characterize the observed measurements [Fig. 6 (red symbols and lines) and Fig. 7]. The estimated binding dissociation constant (K_D) was 0.12 nM, which is in accordance with the in vitro K_D value (0.10 nM). The estimated

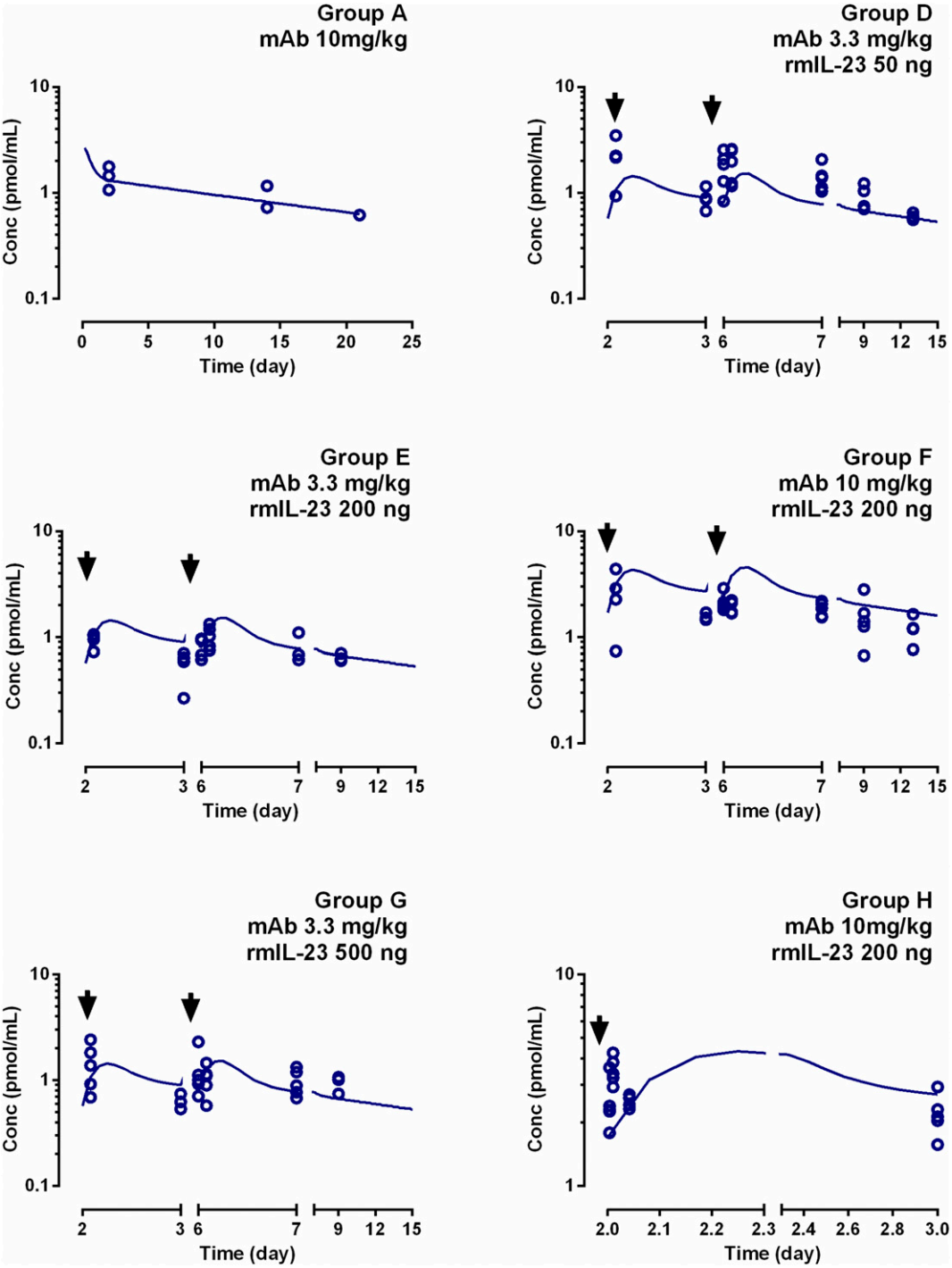

Fig. 5. Model-fitted CNTO 3723 concentrations vs. time profiles in ear homogenates. Circles are measured concentrations and curves depict model fittings.

elimination rate constant of the CNTO 3723-rmIL-23 binding complex in serum (k_{int}) was 0.64, which was ~7-fold higher than serum elimination rate of CNTO 3723 (serum clearance 0.0708 ml/day translates to elimination rate constant 0.083 day^{-1}).

Translational PK/PD Prediction of Ustekinumab Efficacy in Clinical Studies

To examine the potential utility of the developed mechanism-based mPBPK model in translational PK/PD, simulations of IL-23 neutralization profiles following ustekinumab treatment in psoriatic patients in various clinical studies were performed and compared with the reported clinical data. Ustekinumab binds to the common p40 subunit of IL-12 and IL-23. Given the low abundance of endogenous IL-12, the model assumed that IL-12 does not interfere with the interaction between ustekinumab and IL-23. The model also assumed that the distribution kinetics of CNTO 3723 in the ear skin in IL-23-induced PsL mice is comparable with

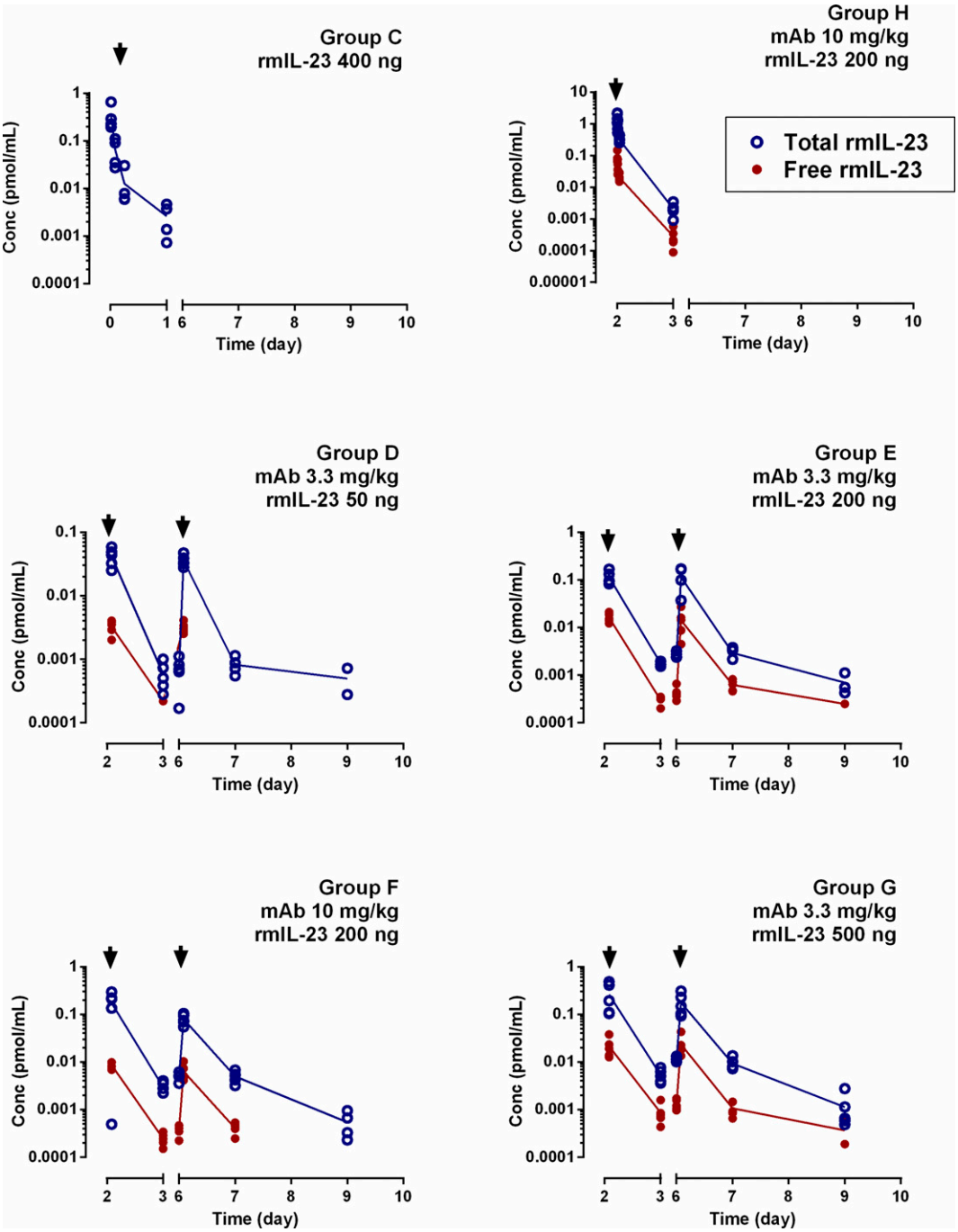

Fig. 6. Model-fitted rmIL-23 concentrations vs. time profiles in ear homogenates. Blue circles are measured total rmIL-23 concentrations, red circles are measured free rmIL-23 concentrations, curves depict model fittings, and arrows indicate the first and last rmIL-23 administration.

that of ustekinumab in the lesional skin site in psoriatic patients since both mAbs have similar size and molecular structure and human and mouse, despite having different skin counterparts (Kawamata et al., 2003), share similar vascular and interstitial tissue structure.

Model simulations were performed under various of scenarios: 1) ustekinumab given once weekly subcutaneously at 90 mg for 4 weeks as reported in a phase II clinical study (Reddy et al., 2010); 2) ustekinumab given as a single subcutaneous dose at 0.27, 0.675, 1.35, or 2.7 mg/kg as reported in a phase I clinical study (Gottlieb et al., 2007); and 3) ustekinumab 45 mg s.c. at 0 and 4 weeks initially, followed by 45 mg s.c. every 12 weeks as a clinically recommended therapeutic dose for psoriatic patients weighing less than 100 kg. Related parameter values for model simulation are listed in Table 3. The model-simulated total IL-23 concentration profiles in serum were compared with the observed data, and the model-simulated free IL-23 concentration profiles in the lesional skin compartment were compared with the reported pharmacological effect in psoriatic patients (Gottlieb et al., 2007; Reddy et al., 2010).

In the first scenario, the model-simulated total IL-23 concentration profile was in good agreement with the measured IL-23 concentrations at different time points (Fig. 8).

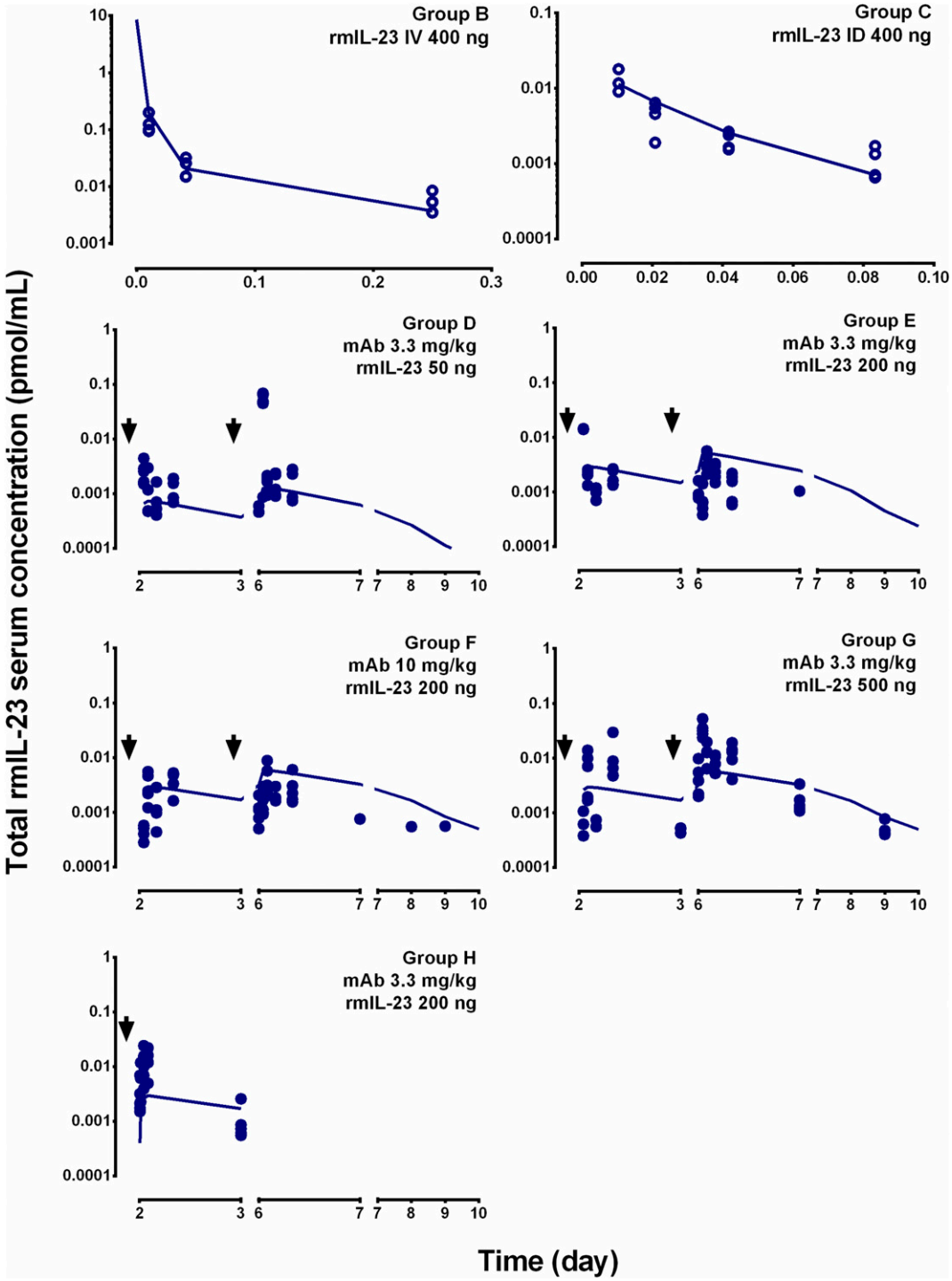

Fig. 7. Model-fitted rmIL-23 concentrations vs. time profiles in serum. Blue circles are measured total rmIL-23 concentrations, curves depict model fittings, and arrows indicate the first and last rmIL-23 administration.

Following the escalating doses of ustekinumab (scenario 2), the model-predicted free IL-23 concentration profiles in lesional skin in psoriatic patients were compared with clinically observed improvements in the psoriasis area and severity index scores as depicted in a phase I clinical study (Gottlieb et al., 2007). Interestingly, the durations of free IL-23 suppression below the threshold of the IL-23 baseline in healthy subjects were in accordance with the duration of sustained improvements in the psoriasis area and severity index scores, despite the small patient sample size and relatively large data variability. Finally, the model simulated the concentration profiles of free IL-23 in serum and lesional skin sites in psoriatic patients following the clinically recommended dose. Free IL-23 in the lesional skin site was suppressed below the threshold of the IL-23 baseline of healthy subjects during the entire time course (Fig. 9). However, on the other hand, free IL-23 in serum was suppressed to a lesser extent and returned to the baseline level in psoriasis patients

TABLE 3
Model parameters for simulation

Parameter	Definition	Value
Ustekinumab serum PK[a]		
k_a (1/day)	First-order absorption rate constant following subcutaneous administration	0.354
V/F (l)	Apparent volume of distribution	15.7
CL/F (l/day)	Apparent clearance	0.465
Ustekinumab tissue distribution kinetics[b]		
σ_{skin}	Vascular reflection coefficient of lesional skin sites	0.742
σ_L	Lymph reflection coefficient of lesional skin sites	0.2
k_{skin} (1/day)	Lymph flow turnover rate of skin	1.4
IL-23 baseline concentration[a]		
$C_{s\ IL23b}$ (pg/ml)	Serum baseline concentration of IL-23 in psoriatic patients	38.5
$C_{Hs\ IL23b}$ (pg/ml)	Serum baseline concentration of IL-23 in healthy subjects	24
$C_{t\ IL23b}$ (pg/ml)	Skin baseline concentration of IL-23 in psoriatic patients	2200
$C_{Ht\ IL23b}$ (pg/ml)	Skin baseline concentration of IL-23 in healthy subjects	936
Ustekinumab interaction with IL-23[b]		
$k_{s\ deg}$ (1/day)	Serum degradation rate constant of IL-23	39.8
$k_{s\ syn}$ (nM/day)	Serum synthesis rate of IL-23	0.028
$k_{s\ int}$ (1/day)	Elimination rate constant of complex in serum	0.15
$k_{t\ deg}$ (1/day)	Skin degradation rate constant of IL-23	2.8
$k_{t\ syn}$ (nM/day)	Skin synthesis rate of IL-23	0.112
$k_{t\ int}$ (1/day)	Elimination rate constant of complex in skin	1.4

[a]Parameter values obtained from El Hadidi et al. (2008) and Zhu et al. (2010).
[b]Parameter values estimated based on allometric scaling from mice: σ_{skin} and σ_L assumed the same from mice; k_{skin} and $k_{s\ deg}$ allometrically scaled from mice with exponent factor −0.25; $k_{t\ deg}$ assumed 2-fold of skin lymph turnover rate (k_{skin}) (Chen et al., 2016); $k_{s\ syn}$ and $k_{t\ syn}$ calculated by multiplying degradation rate constant with IL-23 baseline concentrations; $k_{s\ int}$ assumed 7-fold of ustekinumab elimination rate constant (CL/V) based on model fitting exercise; and $k_{t\ int}$ assumed the same with skin lymph turnover rate (k_{skin}) (Chen et al., 2016).

before the next dose. This suggests that IL-23 concentration in the lesional skin site correlated better with ustekinumab therapeutic efficacy.

Discussion

The mAbs targeting immune cytokines are one of the most successful classes of therapeutic biologics developed for treatment of psoriasis (Tzu et al., 2008). For mAbs targeting soluble cytokines, free target suppression at the tissue site of action is anticipated to be a driver for all downstream pharmacologic effects and therapeutic efficacy, and thus can be a highly valuable translational biomarker. However, free cytokine levels can be technically difficult to determine, especially for the ones with low baseline or function at tissue sites. Moreover, free cytokine suppression at tissue sites cannot be simply extrapolated from that in blood since both the cytokines and mAbs targeting them are expected to exhibit entirely different kinetics at tissue sites and in blood.

To understand target engagement for mAbs against cytokine function at tissue sites, a mechanism-based mPBPK model with TMDD features incorporated in both serum and ear skin was developed to characterize the relationship between CNTO 3723 and rmIL-23 in an IL-23-induced PsL mouse model. The translational utility of this model was examined using ustekinumab. The mPBPK model derived mAb and IL-23 tissue distribution and kinetics parameters were combined with other system- and drug-specific properties such as IL-23 baseline in psoriatic patients, ustekinumab human PK, and IL-23 binding affinity for ustekinumab to predict free IL-23 suppression in skin lesion in psoriatic patients. The results corroborated reasonably well with the observed clinical data, demonstrating the potential of our approach in translational research at the preclinical-clinical interface.

The mPBPK model in PsL mice was developed in a stepwise process that quantitatively delineates each step in the causal chain of the exposure-response relationship of CNTO 3723 and IL-23 at the tissue site of action: 1) tissue distribution of CNTO 3723 to the lesional skin sites, 2) IL-23 dynamics at the lesional skin sites, 3) IL-23 binding and disposition at the target tissue site, and 4) free IL-23 suppression in the lesional skin. Development of a mPBPK model with TMDD features in both blood and tissue requires measurements of the CNTO 3723 and free/total IL-23 concentrations. Endogenous IL-23 is expressed at extremely low levels, i.e., below the limit of quantification of all known bioanalytical methods, making it challenging to study endogenous IL-23 target engagement. To overcome this challenge, exogenously administered rmIL-23 was used. Repeated intradermal administration of rmIL-23 in mice not only led to establishment of a PsL mouse model, it

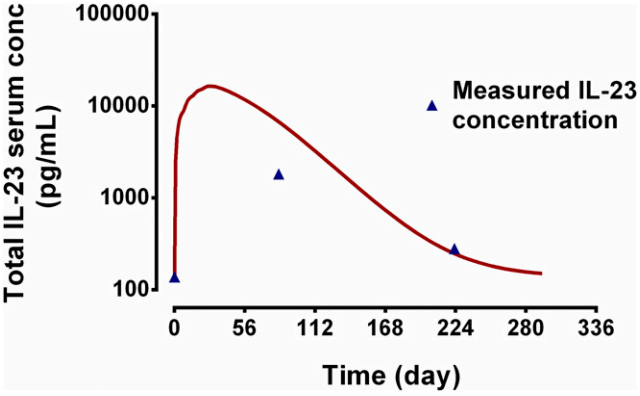

Fig. 8. Model predicted total IL-23 concentration-time profiles in serum overlaid with measured IL-23 serum concentrations following subcutaneous administration of ustekinumab given once weekly for 4 weeks. Triangles are measured IL-23 serum concentrations and curves depict model predictions.

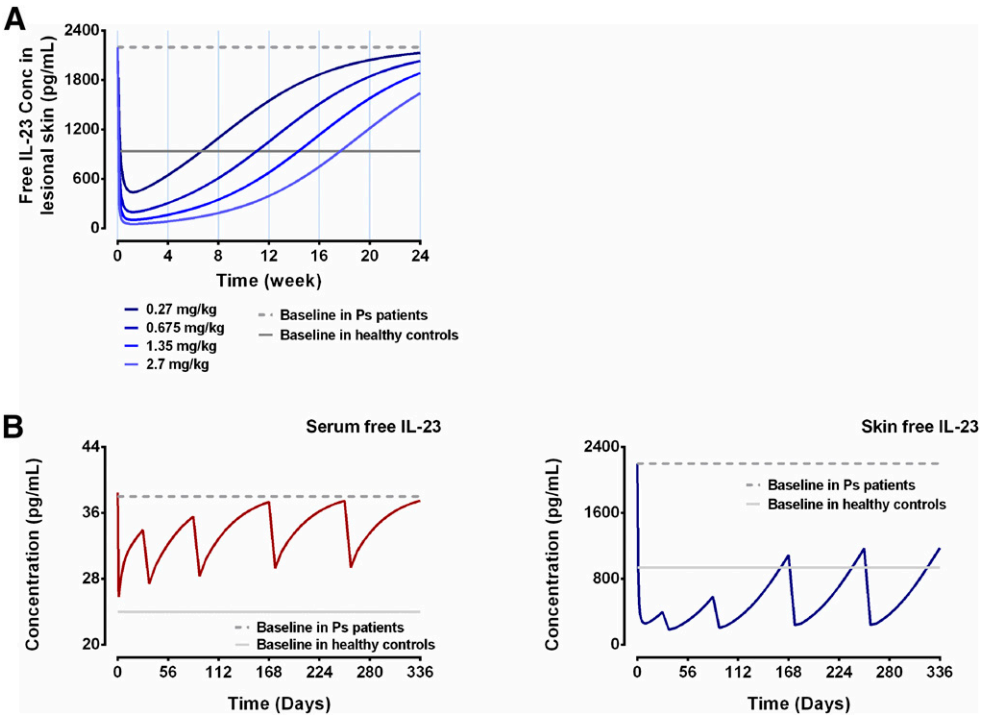

Fig. 9. (A) Model predicted free IL-23 concentration-time profiles in lesional skin following single escalating subcutaneous administration overlaid with measured IL-23 serum concentrations following subcutaneous administration of ustekinumab (placebo, 0.27, 0.675, 1.35, and 2.7 mg/kg). Curves represent model predictions and dashed and solid gray lines are baseline concentrations of IL-23 in psoriatic patients and healthy subjects. (B) Model predicted free IL-23 concentration-time profiles in serum and lesional skin following clinical recommended therapeutic dose (45 mg s.c. at 0 and 4 weeks initially, followed by 45 mg s.c. every 12 weeks). Curves depict model predictions and dashed and solid gray lines are baseline concentrations of IL-23 in psoriatic patients and healthy subjects in serum and lesional skin.

also boosted rmIL-23 baseline concentrations in both serum and ear skin tissues to enable the measurement of rmIL-23 target engagement. Even though rmIL-23 levels in this model are not physiologic, they allow us to characterize the physiologic processes including mAb disposition, IL-23 kinetics, and the interaction between mAb and IL-23. The information can then be integrated with the physiologic levels of IL-23 in psoriatic patients to predict therapeutic effect of anti-IL-23 mAbs in humans.

Interestingly, our results showed that free IL-23 suppression at tissue sites can be more effective than that in blood despite the lower mAb level and higher IL-23 level at the tissue site. This can be attributed to the substantially lower mAb-IL-23 complex accumulation at the tissue site. In blood, IL-23 is subject to rapid elimination (half-life in minutes) while the mAb-IL-23 complex is eliminated much slower (half-life in days, similar to that of IgG). This leads to a rapid accumulation of total IL-23 in blood after mAb dosing. The mAb-IL-23 complex would dissociate and form a new equilibrium between mAb and free IL-23, resulting in return of free IL-23 to baseline level when the mAb concentrations are still orders of magnitude higher (Wang et al., 2014). On the other hand, free IL-23 and the mAb-IL-23 complex have similar elimination rates (close to that of lymph drainage) at the tissue site and there is minimal accumulation of the mAb-IL-23 complex, resulting in more effective free IL-23 suppression in the ear skin.

In our mPBPK model, the pharmacokinetics of rmIL-23 and CNTO 3723 were characterized with the first- and second-generation mPBPK model, respectively (Cao and Jusko, 2012; Cao et al., 2013). Compared with mAbs, rmIL-23 exhibits more rapid and extensive tissue distribution. The first-generation mPBPK model, which assumes that whole tissue weight or tissue interstitial space as the extravascular distribution space and tissue distribution is driven by Fick's laws of diffusion, was found to be more suitable for describing the disposition of rmIL-23. The second-generation mPBPK model was developed with considerations of specific PK characteristics of mAbs, i.e., only convection was considered as the driver for extravascular distribution, and only ISF was considered as the extravascular distribution space, and it was used to describe the disposition of CNTO 3723. Importantly, both the first- and second-generation mPBPK models used physiologic volumes and flows, and thus could be easily integrated for assessing the interrelationship between CNTO 3723 and IL-23.

A vascular endothelial endosome space and neonatal Fc receptor FcRn-mAb interaction are frequently included in physiologically based pharmacokinetic models for mAbs to assess the influence of FcRn interaction (Garg and Balthasar, 2007; Chetty et al., 2015). Since our interest focused on understanding the target engagement at the tissue site of action, not the impact of FcRn binding, these parameters were not included in our mPBPK model. It should be noted that the overall volume of vascular endothelial endosomes was only about 0.4% of plasma and less than 0.1% of ISF volume (Cao et al., 2013), thus the contribution of mAbs residing within this space to overall mAb disposition is expected to be limited at any moment of time. In addition, FcRn-mediated clearance (i.e., salvage of mAbs following their pinocytosis) and extravascular distribution are both linear processes unless the mAb concentrations are greater than ~10 mg/ml (Roopenian and Akilesh, 2007). Therefore, the linear serum clearance and extravascular distribution functions implemented in our mPBPK model would implicitly include these FcRn-mediated mechanisms.

Two important physiologic determinants that describe the distribution kinetics of CNTO 3723 into ear skin are the transvascular fluid flux rate, which would equal the lymph flow rate (L) based on fluid mass balance, and vascular

permeability (σ). Lymph flow rate is commonly determined through lymph node cannulation, but skin is the largest organ that covers the entire body and the skin lymph flow rate cannot be assessed directly. Instead of the lymph flow rate, the lymph turnover rate of skin (k_{ear}) was applied, where k_{ear} is defined as L divided by the ISF volume (V_{ISF}), which could be measured experimentally by tracing the removal rate of radioactive-labeled albumin (Reed et al., 1985). The estimated regular intradermal absorption rate constant of rmIL-23 is also comparable with the reported skin lymph turnover rate, suggesting the regular intradermal absorption pathway for IL-23 is predominantly lymph uptake. Besides the regular intradermal absorption, the absorption of rmIL-23 following intradermal injection was also impacted by blister formation. Similar to that following subcutaneous administration, large-molecule absorption following intradermal injection is driven by the differences in hydrostatic and osmotic pressure between blood circulation, interstitium, and the lymphatic vessels (Wiig and Swartz, 2012). Blisters formed due to repeated intradermal injection of rmIL-23 increase hydrostatic pressure in the interstitium, which might cause rapid absorption of rmIL-23 into capillaries. It has been observed that intradermal administration of proteins produced higher maximum serum concentration (C_{max}) and a left shift in serum concentration profiles compared to the subcutaneous route (Milewski et al., 2015).

For our PsL mice study, it was unexpected to find that repeated intradermal administration of a relatively large volume of rmIL-23 to the mouse ears led to certain pathophysiological changes that affected the pharmacokinetics of CNTO 3723 as well as rmIL-23. This presented challenges in directly using results from the PsL mouse model for human dose projection because such effects are not expected to happen in humans. One advantage of using a mechanism and physiologically based model is that the model can be expanded with additional components corresponding to possible physiologic explanations to capture the observed data for CNTO 3723 and IL-23 in both serum and skin. Since the model distinguished the effects from physiological and nonphysiological processes, only the physiologic process was used for human dose projection.

In conclusion, we provided a good case example of how mechanism and physiologically based modeling and simulations can be applied during early drug discovery and preclinical to clinical translational stages. Simple extrapolation of drug exposure-efficacy relationships from preclinical species to human likely will not work due to the interspecies differences in disease status, target kinetics, and drug disposition. In particular, tissue-specific drug and target kinetics information must be considered to understand target suppression at the tissue site of action. Physiologically based PK/PD modeling can be an invaluable tool, which can be used to understand system-specific and drug-specific physiologic parameters and enable successful translation from preclinical models to humans.

Acknowledgments

We thank Natasha Rozenkrants for helping to establish the IL-23-induced PsL model, and Dr. Yang Wang for helping in the management of the in-life study conducted at WuXi Apptec.

Authorship Contributions

Participated in research design: Chen, Jiang, Zhou, Wang.

Conducted experiments: Chen, Doddareddy, Geist, McIntosh, Wang.

Contributed new reagents or analytic tools: Chen, Doddareddy, Geist, McIntosh.

Performed data analysis: Chen, Jiang, Zhou, Wang.

Wrote or contributed to the writing of the manuscript: Chen, Jiang, Doddareddy, Geist, McIntosh, Jusko, Zhou, Wang.

References

Agoram BM, Martin SW, and van der Graaf PH (2007) The role of mechanism-based pharmacokinetic-pharmacodynamic (PK-PD) modelling in translational research of biologics. *Drug Discov Today* **12**:1018–1024.

Aldrich MB and Sevick-Muraca EM (2013) Cytokines are systemic effectors of lymphatic function in acute inflammation. *Cytokine* **64**:362–369.

Arican O, Aral M, Sasmaz S, and Ciragil P (2005) Serum levels of TNF-α, IFN-γ, IL-6, IL-8, IL-12, IL-17, and IL-18 in patients with active psoriasis and correlation with disease severity. *Mediators Inflamm* **2005**:273–279.

Cao Y, Balthasar JP, and Jusko WJ (2013) Second-generation minimal physiologically-based pharmacokinetic model for monoclonal antibodies. *J Pharmacokinet Pharmacodyn* **40**:597–607.

Cao Y and Jusko WJ (2012) Applications of minimal physiologically-based pharmacokinetic models. *J Pharmacokinet Pharmacodyn* **39**:711–723.

Cao Y and Jusko WJ (2014) Incorporating target-mediated drug disposition in a minimal physiologically-based pharmacokinetic model for monoclonal antibodies. *J Pharmacokinet Pharmacodyn* **41**:375–387.

Chan JR, Blumenschein W, Murphy E, Diveu C, Wiekowski M, Abbondanzo S, Lucian L, Geissler R, Brodie S, Kimball AB, et al. (2006) IL-23 stimulates epidermal hyperplasia via TNF and IL-20R2-dependent mechanisms with implications for psoriasis pathogenesis. *J Exp Med* **203**:2577–2587.

Chen X, Jiang X, Jusko WJ, Zhou H, and Wang W (2016) Minimal physiologically-based pharmacokinetic (mPBPK) model for a monoclonal antibody against interleukin-6 in mice with collagen-induced arthritis. *J Pharmacokinet Pharmacodyn* **43**:291–304.

Chetty M, Li L, Rose R, Machavaram K, Jamei M, Rostami-Hodjegan A, and Gardner I (2015) Prediction of the pharmacokinetics, pharmacodynamics, and efficacy of a monoclonal antibody, using a physiologically based pharmacokinetic FcRn model. *Front Immunol* **5**:670.

Danhof M, de Jongh J, De Lange EC, Della Pasqua O, Ploeger BA, and Voskuyl RA (2007) Mechanism-based pharmacokinetic-pharmacodynamic modeling: biophase distribution, receptor theory, and dynamical systems analysis. *Annu Rev Pharmacol Toxicol* **47**:357–400.

Dong J and Goldenberg G (2017) New biologics in psoriasis: an update on IL-23 and IL-17 inhibitors. *Cutis* **99**:123–127.

Dragatin C, Polus F, Bodenlenz M, Calonder C, Aigner B, Tiffner KI, Mader JK, Ratzer M, Woessner R, Pieber TR, et al. (2016) Secukinumab distributes into dermal interstitial fluid of psoriasis patients as demonstrated by open flow microperfusion. *Exp Dermatol* **25**:157–159.

Eigenmann MJ, Karlsen TV, Krippendorff BF, Tenstad O, Fronton L, Otteneder MB, and Wiig H (2017) Interstitial IgG antibody pharmacokinetics assessed by combined in vivo- and physiologically-based pharmacokinetic modelling approaches. *J Physiol* **595**:7311–7330.

El Hadidi H, Grace BDM, Gheita T, and Shaker O (2008) Involvement of IL-23 in psoriasis and psoriatic arthritis patients; possible role in pathogenesis. *J Egypt worn Dermatol Soc* **5**:70–76.

Garg A and Balthasar JP (2007) Physiologically-based pharmacokinetic (PBPK) model to predict IgG tissue kinetics in wild-type and FcRn-knockout mice. *J Pharmacokinet Pharmacodyn* **34**:687–709.

Gibiansky L, Gibiansky E, Kakkar T, and Ma P (2008) Approximations of the target-mediated drug disposition model and identifiability of model parameters. *J Pharmacokinet Pharmacodyn* **35**:573–591.

Gottlieb AB, Cooper KD, McCormick TS, Toichi E, Everitt DE, Frederick B, Zhu Y, Pendley CE, Graham MA, and Mascelli MA (2007) A phase 1, double-blind, placebo-controlled study evaluating single subcutaneous administrations of a human interleukin-12/23 monoclonal antibody in subjects with plaque psoriasis. *Curr Med Res Opin* **23**:1081–1092.

Hu C, Wasfi Y, Zhuang Y, and Zhou H (2014) Information contributed by meta-analysis in exposure-response modeling: application to phase 2 dose selection of guselkumab in patients with moderate-to-severe psoriasis. *J Pharmacokinet Pharmacodyn* **41**:239–250.

Ibrahim R, Nitsche JM, and Kasting GB (2012) Dermal clearance model for epidermal bioavailability calculations. *J Pharm Sci* **101**:2094–2108.

Kawamata S, Ozawa J, Hashimoto M, Kurose T, and Shinohara H (2003) Structure of the rat subcutaneous connective tissue in relation to its sliding mechanism. *Arch Histol Cytol* **66**:273–279.

Kopp T, Lenz P, Bello-Fernandez C, Kastelein RA, Kupper TS, and Stingl G (2003) IL-23 production by cosecretion of endogenous p19 and transgenic p40 in keratin 14/p40 transgenic mice: evidence for enhanced cutaneous immunity. *J Immunol* **170**:5438–5444.

Lima HC and Kimball AB (2010) Targeting IL-23: insights into the pathogenesis and the treatment of psoriasis. *Indian J Dermatol* **55**:171–175.

Lowes MA, Russell CB, Martin DA, Towne JE, and Krueger JG (2013) The IL-23/T17 pathogenic axis in psoriasis is amplified by keratinocyte responses. *Trends Immunol* **34**:174–181.

Milewski M, Manser K, Nissley BP, and Mitra A (2015) Analysis of the absorption kinetics of macromolecules following intradermal and subcutaneous administration. *Eur J Pharm Biopharm* **89**:134–144.
Nestle FO, Kaplan DH, and Barker J (2009) Psoriasis. *N Engl J Med* **361**:496–509.
Reddy M, Torres G, McCormick T, Marano C, Cooper K, Yeilding N, Wang Y, Pendley C, Prabhakar U, Wong J, et al. (2010) Positive treatment effects of ustekinumab in psoriasis: analysis of lesional and systemic parameters. *J Dermatol* **37**:413–425.
Reed RK, Johansen S, and Noddeland H (1985) Turnover rate of interstitial albumin in rat skin and skeletal muscle. Effects of limb movements and motor activity. *Acta Physiol Scand* **125**:711–718.
Rizzo HL, Kagami S, Phillips KG, Kurtz SE, Jacques SL, and Blauvelt A (2011) IL-23-mediated psoriasis-like epidermal hyperplasia is dependent on IL-17A. *J Immunol* **186**:1495–1502.
Roopenian DC and Akilesh S (2007) FcRn: the neonatal Fc receptor comes of age. *Nat Rev Immunol* **7**:715–725.
Schön MP and Boehncke WH (2005) Psoriasis. *N Engl J Med* **352**:1899–1912.
Shah DK and Betts AM (2012) Towards a platform PBPK model to characterize the plasma and tissue disposition of monoclonal antibodies in preclinical species and human. *J Pharmacokinet Pharmacodyn* **39**:67–86.
Tzu J, Krulig E, Cardenas V, and Kerdel FA (2008) Biological agents in the treatment of psoriasis. *G Ital Dermatol Venereol* **143**:315–327.
Vieira P and Rajewsky K (1988) The half-lives of serum immunoglobulins in adult mice. *Eur J Immunol* **18**:313–316.
Wang W, Wang X, Doddareddy R, Fink D, McIntosh T, Davis HM, and Zhou H (2014) Mechanistic pharmacokinetic/target engagement/pharmacodynamic (PK/TE/PD) modeling in deciphering interplay between a monoclonal antibody and its soluble target in cynomolgus monkeys. *AAPS J* **16**:129–139.
Wiig H and Swartz MA (2012) Interstitial fluid and lymph formation and transport: physiological regulation and roles in inflammation and cancer. *Physiol Rev* **92**: 1005–1060.
Zhou H, Hu C, Zhu Y, Lu M, Liao S, Yeilding N, and Davis HM (2010) Population-based exposure-efficacy modeling of ustekinumab in patients with moderate to severe plaque psoriasis. *J Clin Pharmacol* **50**:257–267.
Zhu YW, Mendelsohn A, Pendley C, Davis HM, and Zhou H (2010) Population pharmacokinetics of ustekinumab in patients with active psoriatic arthritis. *Int J Clin Pharmacol Ther* **48**:830–846.

Address correspondence to: Dr. Weirong Wang, Biologics Development Sciences, Janssen BioTherapeutics, Janssen R&D, 1400 McKean Road, Spring House, PA 19447. E-mail: wwang83@its.jnj.com